Scuola IMT Alti Studi Lucca

Statistical physical theory of mode-locking laser generation with a frequency comb

Questa è la versione preprint della seguente opera:

Original
Statistical physical theory of mode-locking laser generation with a frequency comb / Antenucci, F., Ibáñez Berganza, M., Leuzzi, L.. - In: PHYSICAL REVIEW A. - ISSN 1050-2947. - 91:4(2015). [10.1103/PhysRevA.91.043811]

Availability:
This version is available at: 20.500.11771/25014

Publisher:

Published
DOI:10.1103/PhysRevA.91.043811

Terms of use:

This publication is made accessible in accordance with the terms for deposit in the institutional repository, as defined by the IMT School for Advanced Studies Lucca's Open Access Policy. (https://library.imtlucca.it/sites/default/files/regolamento-policy-open-access-imtlib_0.pdf).

Si prega di consultare le pagine informative dell'editore relative alle politiche di autoarchiviazione.

(Article begins on next page)

09 November 2026

Statistical physical theory of mode-locking laser generation with a frequency comb

F. Antenucci[1,2], M. Ibáñez Berganza[3], L. Leuzzi[1,2]
[1] *NANOTEC-CNR, Institute of Nanotechnology, Soft and Living Matter Laboratory, Rome, Piazzale Aldo Moro 5, I-00185, Roma, Italy*
[2] *Dipartimento di Fisica, Università di Roma "Sapienza,"Piazzale Aldo Moro 5, I-00185, Roma, Italy*
[3] *INFN, Gruppo Collegato di Parma, via G.P. Usberti, 7/A - 43124, Parma, Italy*

A study of the Mode-locking lasing pulse formation in closed cavities is presented within a statistical mechanical framework where the onset of laser coincides with a thermodynamic phase transition driven by the optical power pumped into the system. Electromagnetic modes are represented by classical degrees of freedom of a Hamiltonian model at equilibrium in an effective ensemble corresponding to the stationary laser regime. By means of optimized Monte Carlo numerical simulations, the system properties are analyzed varying mode interaction dilution, gain profile and number of modes. Novel properties of the resulting mode-locking laser phase are presented, not observable by previous approaches based on mean-field approximations. For strong dilution of the nonlinear interaction network, power condensation occurs as the whole optical intensity is taken by a few electromagnetic modes, whose number does not depend on the size of the system. For all reported cases laser thresholds, intensity spectra, phase waves and ultra-fast electromagnetic pulses are computed.

arXiv:1409.6345v2 [physics.optics] 23 Apr 2015

I. INTRODUCTION

In multimode lasers with many cavity modes, nonlinear interactions originate among modes. One notable mechanism inducing interaction is saturable absorption, i.e., the progressive depletion of low power tails of the light pulse traveling through the cavity at each roundtrip. This causes the consequent amplification of very short pulses composed by modes with *locked phases*, a phenomenon called *mode-locking* [1, 2]. Mode-locking (ML) derives from the nonlinear synchronization constraint on the oscillations of interacting modes. Given any quadruplet of modes $\{k_1, k_2, k_3, k_4\}$ this is expressed by the frequency matching condition (FMC):

$$|\nu_{k_1} - \nu_{k_2} + \nu_{k_3} - \nu_{k_4}| \leq \gamma \ . \tag{1}$$

where γ is the single mode line-width. Phase-locking occurs at the ML lasing threshold and corresponds to some long-range order in the set of modes in the cavity.

We adopt a statistical mechanical approach to describe the optical properties of stimulated light emission from cavities with a large number of modes. In this approach the generation of a multimode ML lasing regime from a fluorescent continuous wave (CW) regime as the optical power in the cavity is increased can be characterized as a thermodynamic phase transition between a disordered phase and a phase with long-range order . The stationary laser system can be treated as a thermodynamic system at equilibrium in a thermal bath whose effective temperature is proportional to the inverse squared power pumped into the cavity [3, 4]. Since the first attempt by Gordon and Fischer in the early 00's [5], this approach has been performed in a mean-field fully connected approximation corresponding in the optical language to the so-called *narrow-band approximation*, see also Refs. [3, 6–8]. This consists in choosing mode frequencies in a narrow bandwidth $\Delta\nu$ around the central frequency of the cavity. So narrow that the frequency interspacing $\delta\nu$ between resonant modes is less than the linewidth γ of each mode. In this way Eq. (1) is practically always satisfied and, therefore, actually irrelevant in determining lasing properties.

In the present work we introduce frequency dependent populations of modes, considering gain profiles $g(\nu)$ and the effect of nontrivial frequency matching on the mode couplings. This analysis requires to go beyond the limits of validity of mean-field theory and it is carried out by means of optimized Monte Carlo (MC) simulations running on GPU's. An exhaustive numerical analysis accounting for the fluctuations induced by these new ingredients reveals that, depending on the optical system properties, on the cavity topology, and on the relative gain-to-nonlinearity strength, different thermodynamic-like phases occur. Such regimes range from a ferromagnetic-like one, where all mode phases are aligned, to a *phase-wave* one, where phases of modes at nearby frequencies are strongly correlated, though not equal to each other. The ferromagnetic behavior occurs in the low finesse limit of the narrowband approximation. Non-trivial phase locking occurs, instead, at high finesse. In the latter case we show how, distributing the frequencies according to an optical frequency comb [9–11], intensity spectra and pulse phase delay observed in ultra-short pulses are reproduced [12].

As it will be taken up in the following, previous studies based on mean-field theory are exact only in the narrow band-width case. In this paper we go beyond the mean-field approximation, accounting also for situations in which different modes exhibit different frequencies

Our study introduces two essential and new ingredients. The first one is the FMC, yielding mode interaction networks that are no longer described by mean-field theory, in which non-trivial multimode emission spectra and mode phase correlations above threshold occur. The second ingredient is a *random* dilution of the interacting network, modeling possible topological disorder in arbitrary cavity structures, as, e.g., multi cavity channels not exactly equal to each other. We will show that, as far as

it is not too strong, the latter kind of dilution does not alter at all the laser transition properties. Below a certain dilution point, however, in the lasing phase the whole optical power condenses into a small set of connected modes, scaling independently of the number of modes.

II. THE MODEL

Expanding the electromagnetic field in the complete base of N normal modes $\{\boldsymbol{E}_n(\boldsymbol{r}), \nu_n\}$[13]

$$\boldsymbol{E}(\boldsymbol{r},t) = \sum_{n=1}^{N} a_n(t) e^{-2\pi\imath\nu_n t} \boldsymbol{E}_n(\boldsymbol{r}) + \text{c.c.} \qquad (2)$$

the equilibrium dynamics of the time-dependent complex amplitudes $a_n(t)$ is given by the Hamiltonian [5]

$$\mathcal{H} = -\sum_{k=1}^{N} g_k |a_k|^2 - J \sum_{\{k_1,k_2,k_3,k_4\}}^{\text{ML}} a_{k_1} a^*_{k_2} a_{k_3} a^*_{k_4} \qquad (3)$$

where g_k and J are chosen as real numbers, neglecting dispersion and Kerr-lens effect. The physical meaning of the coefficients comes from the equivalence of the Hamiltonian dynamical equation with the Haus master equation [1]: $g_k = g(\nu_k)$ is the net gain profile, J is the self-amplitude modulation (SAM) coefficient. The ML sum runs over a subset of quadruplets such that for each element (k_1, k_2, k_3, k_4) the FMC holds. The latter implies that in the non-linear term of Eq. (3) three non-equivalent orderings of quadruplets contribute to the sum, each one consisting of eight equivalent index permutations [38]. The Hamiltonian is symmetrized with respect to these orderings. The coupling strength in Eq. (3) is taken as $J = N/N_q$, where N_q is the number of quadruplets, making the Hamiltonian extensive.

The total optical energy stored in the system is $\mathcal{E} = N\epsilon = \sum_{k=1}^{N} |a_k|^2$ and it is kept constant in the dynamics by external power pumping. Eq. (3) is a direct generalization of the Hamiltonian studied in Ref. [5] and can be seen as the ordered limit of the random laser theory analyzed in Refs. [3, 7, 8]. From the point of view of statistical mechanics the driven optical system composed by the cavity, the amplifying medium *and* the optical power pumped into the system can be described by Eq. (3), considering it as the Hamiltonian of a system at equilibrium with an effective thermal bath. The role of the inverse temperature is played by the pumping rate squared: $\mathcal{P}^2 = \beta J \epsilon^2$. Here $\beta = 1/k_b T$ is the inverse *heat bath* temperature, regulating spontaneous emission. It is usually represented as white noise in a Langevin dynamics [3–8, 14, 15].

III. MODE INTERACTION NETWORK

Thermodynamic phases are determined by the interaction network, as well. In the following we will undergo the analysis of networks with a varying degree of dilution. This will be expressed as number of quadruplets N_q vs. number of modes N. We will discuss data for $N_q = \mathcal{O}(N^t)$, $t = 1, 2, 3, 4$.

Two essentially different types of topologies will be investigated, depending on the frequency bandwidth being narrow or finite. Both topologies can be further diluted upon homogeneously randomly removing quadruplets. The "Narrow Band-width Topology" (NBT) is *low finesse*, i.e., $\delta\nu \ll \gamma$, and the role of frequencies is irrelevant. The fully connected instance, consisting in $N_q = N(N-1)(N-2)(N-3)/8$ interacting quadruplets, corresponds to a closed Fabry-Perot-like cavity where all longitudinal modes are localized in the same spatial region. Possible random diluted NBT's correspond to more complicated geometries, including multi-channels set-ups. For finite bandwidth, instead, we will work in the *high-finesse* limit, $\delta\nu \gg \gamma$, with sets of equispaced frequencies [9–11, 16, 17]. We will term this a "Frequency Comb Topology" (FCT). In this case the list of quadruplets is extracted from those nontrivially satisfying Eq. 1: modes are not all equivalent to each other and mean-field theory does not hold.

IV. NUMERICAL SIMULATIONS AND DATA ANALYSIS

We performed extensive Monte Carlo simulations of equilibrium dynamics by means of the exchange MC [18] algorithm and the synchronous, fully parallel MC [19–22]. The latter, indeed, remarkably turns out to reproduce a reliable dynamics in the present model [23]. In the NBT, system sizes from $N = 25$ to 500 have been simulated for random dilutions of $N_q = \mathcal{O}(N^t)$, $t = 2, 3, 4$. [39]. For the FCT, we simulated systems of size $N = 100 - 1000$ with number of frequencies $N_f = N$ in each case, and $N_q = \mathcal{O}(N^2)$ and $\mathcal{O}(N^3)$ upon applying the FMC filter.

The gain $g(\nu_n)$ is taken as Gaussian with varying mean square displacement. We checked thermal equilibration, i.e., the onset of the pumped stationary regime, by looking at the energy relaxation and at the symmetry of the distribution of complex amplitude values deep in the lasing phase. In the following we present our results about (I) laser thresholds identification, (II) intensity spectra, and (III) phase waves, electromagnetic pulses and their correlations.

(I) Laser threshold

The estimate of the laser threshold is obtained from the finite size scaling (FSS) analysis of the behavior of the energy vs. pumping rate, as shown in Fig. 1 for the FCT (for the NBT the energy behavior is the same). For low $\mathcal{P}$ the system is in an incoherent continuous wave regime with uncorrelated phases and zero energy per mode. As $\mathcal{P}$ increases a phase transition occurs indicated by a dis-

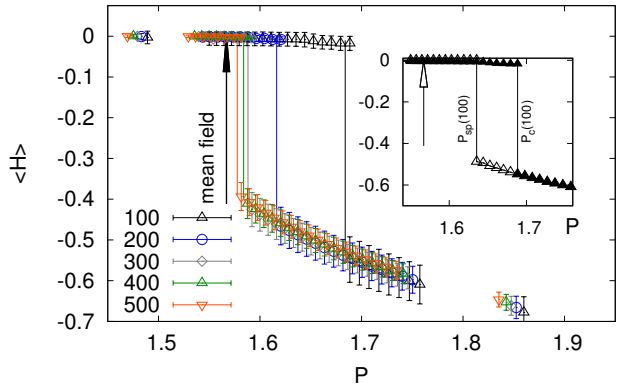

FIG. 1: (Color online) Energy vs. $\mathcal{P}$ (in arbitrary units) in the Frequency Comb case with $N_q \propto N^2$. The arrow marks the analytic critical point in the thermodynamic limit of the NBT. Inset: for $N = N_f = 100$ modes the spinodal line $\mathcal{P}_{\rm sp}$ is shown next to the threshold critical line.

continuity in the energy. For the NBT the $N \to \infty$ critical point is analytically known [3] and pointed out to as an arrow in Fig. 1. For $N_q = \mathcal{O}(N^t)$, $t = 2, 3, 4$ the FSS of the discontinuity point is compatible with the fully connected analytical limit, as reported in Tab. I. The critical thresholds for the FCT case, estimate by FSS for $N_q = \mathcal{O}(N^2)$ and for $N_q = \mathcal{O}(N^3)$ are reported in Tab. I. The CW/ML laser phase transition is first order: in the inset of Fig. 1 both the spinodal and the critical points are displayed, e.g., for $N = 100$ in a FCT. Spinodal points occur both in NBT and in FCT. In Fig. 2 the average mode magnitudes $r \equiv \langle |a| \rangle / \sqrt{\epsilon}$ are plotted. This is $\sqrt{2/\pi}$ for randomly independently oscillating amplitudes and it discontinuously increases at the ML lasing threshold indicating intensity mode-locking. For $\mathcal{P} \to \infty$, r tends to 1 in the NBT and to 0.990(1) in the FCT case.

Power condensation

As the dilution is strong, i.e., $N_q = \mathcal{O}(N)$, each mode interacts in a $\mathcal{O}(1)$ number of quadruplets. Above threshold the whole power $\mathcal{E}$ turns out to be taken by a small number of connected modes and the probability to find a configuration with energy equipartition is negligible in the thermodynamic limit. In the mean field approximation one can prove that in order to display power condensation it must be $N_q < \mathcal{O}(N^2)$ [23] as confirmed by numerical simulations. In the following we focus on more connected networks.

ν band	Narrow Band				Frequency Comb	
$O(N_q)$	N^2	N^3	N^4	Exact	N^2	N^3
$\mathcal{P}_c$	1.56(3)	1.59(9)	1.6(3)	1.56697	1.558(8)	1.57(1)

TABLE I: Critical point for $N \to \infty$ in various dilutions.

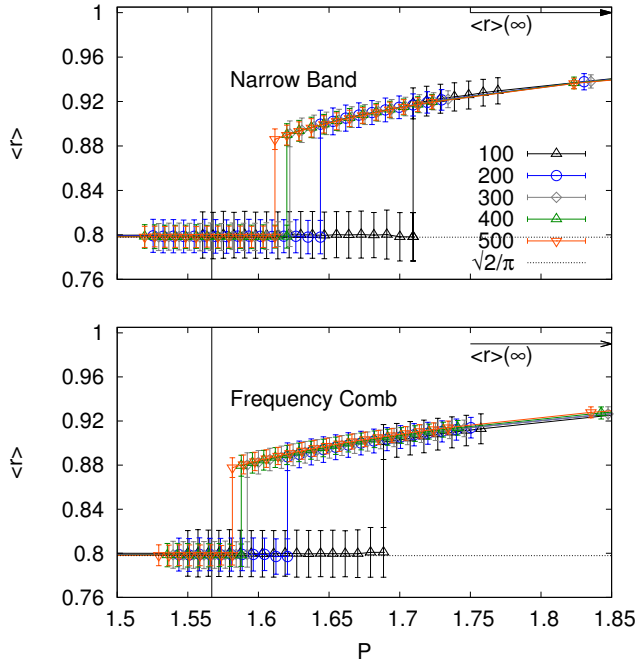

FIG. 2: (Color online) Average mode magnitude $r = \langle |a| \rangle / \sqrt{\epsilon}$ vs. optical power $\mathcal{P}$ (in a. u.) for different sizes in the NBT (top panel) and in the FCT (bottom panel).

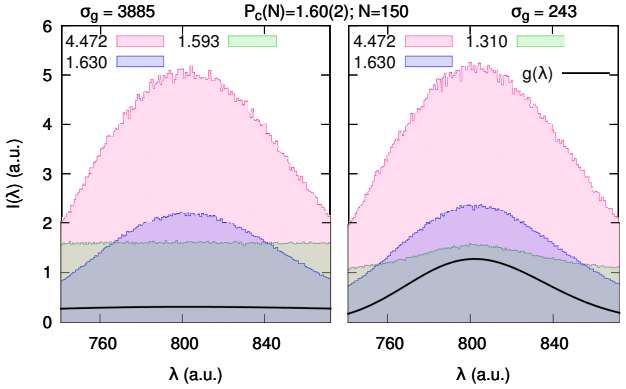

FIG. 3: (Color online) Intensity spectra for a FCT system of $N_f = N = 150$. $N_q = \mathcal{O}(N^2)$ for increasing $\mathcal{P}$ from bottom to top. Left: gain $g(\lambda)$ with larger variance, $\sigma_\lambda = 3885$. At $\mathcal{P} > \mathcal{P}_c$ the spectrum starts narrowing because of the nonlinear mode-coupling. Right: $g(\lambda)$ with smaller variance, $\sigma_\lambda = 243$. Spectra follow the peaked gain profile already in the CW regime. At $\mathcal{P}_c$ mode-locking sets in, enhancing the sharpening.

(II) Intensity spectra

In Fig. 3 we show two instances of the spectra $I(\lambda_j) = \langle |a_j|^2 \rangle$ vs. $\lambda_j = c/\nu_j$ in FCT systems with Gaussian gain profiles with different variances. In the left panel the mean square displacement of the gain profile in the wavelength dominion is large ($\sigma_g = 3885$) in comparison to the

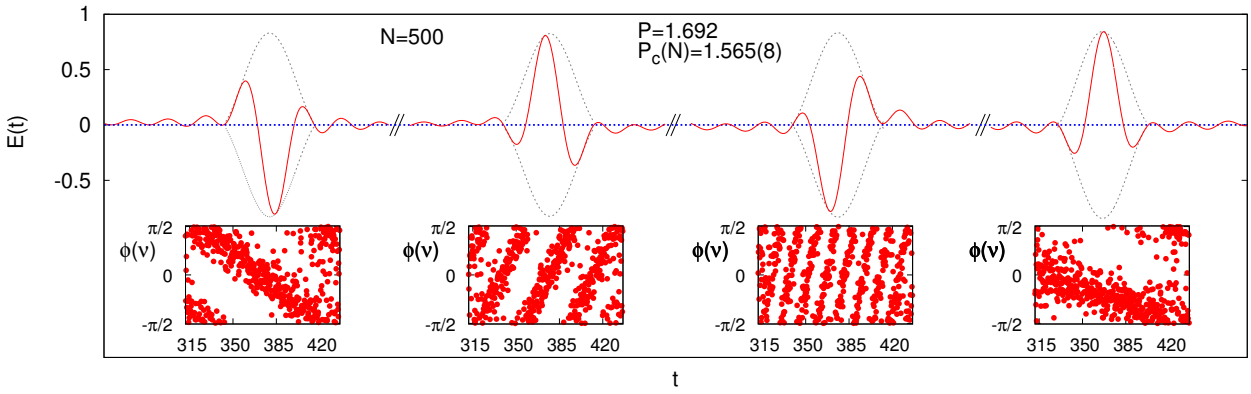

FIG. 4: Electromagnetic field $E(t)$ at different emissions in the system dynamics with a uniform comb distribution for mode frequencies. $N = N_f = 500$. Bottom insets: phase-locked linear behavior $\phi(\nu)$ corresponding to each pulse. The phase shift in the peak of $E(t)$ with respect to the maximum of the envelope corresponds to the slope of $\phi(\nu)$. Time is in arbitrary units.

spectral free range, whereas in the right panel it is of the same order of magnitude ($\sigma_g = 243$). In the first case, below $\mathcal{P}$ the CW spectrum is flat and suddenly sharpens at the ML threshold $\mathcal{P}_c$. To underline this, spectra are shown right below and above $\mathcal{P}_c(N = 150) = 1.597(15)$ in Fig. 3. In the small σ_g case the spectra appears already narrower in the CW regime, following $g(\lambda)$, as displayed in the right panel of Fig. 3 for the lowest simulated pumping rate. At $\mathcal{P}_c$ though, their narrowing qualitatively changes and becomes progressively independent of $g(\lambda)$ as $\mathcal{P}$ increases, eventually taking the same spectral shape of the previous case.

We show in Fig. 3 the cumulative detections of very many pulses, as in data acquisition from ultra-fast ML lasers. In the MC dynamics used in simulation, though, each MC step corresponds to a pulse generation. Within our approach it is, then, possible to look at the dynamics at much shorter time intervals, where the mode amplitude and intensity profile in λ fluctuates from pulse to pulse. This is connected to changes in the spectral phase delay of the electromagnetic pulse. Different spectral dynamics are reported in Video 1 of Sup. Mat. [37] (see details in Sec. VI).

(III) Electromagnetic pulses and phase delay

In terms of slow complex amplitudes, cf. Eq (2), $a_n(\tau) = A_n(\tau)e^{\imath\phi_n(\tau)}$, $A_n = |a_n|$, the electromagnetic pulse is

$$E(t|\tau) = \sum_{n=1}^{N} A_n(\tau)e^{\imath[2\pi\nu_n t+\phi_n(\tau)]} \tag{4}$$

The time $\tau \gg t$ operatively labels a single MC step in our simulations, i.e., the interval between two pulses. In Fig. 4 we show $E(t|\tau)$ at four different times τ in the dynamics. In the NBT, in the ML regime all modes acquire same modulus and phase. In a FCT, instead, at $\mathcal{P}_c$ a non-trivial phase-locking occurs, such that the mode phases exhibit a linear dependence on the mode frequencies: $\phi_n \simeq \phi_0 + \phi'\nu_n$, as shown in the bottom insets of Fig. 4. The pulse is, thus, unchirped [1]. The spectral *phase delay*, or group delay, $\phi' = d\phi(\nu)/d\nu|_{\nu=\nu_n}$ of the optical pulse does not depend on the frequency of mode n. It changes, though, with time τ, from pulse to pulse. Within our approach we thus find the typical spectral phase frequency profile $\phi(\nu)$ at each given pulse and its pulse-to-pulse dynamics, cf. Video 2 in Sup. Mat. [37] (see details in Sec. VI).

Phase waves lifetime

Let us define the time average over an equilibrated set of data ($\tau \geq \tau_{\rm therm}$) on a time window $\mathcal{T}$: $\langle\ldots\rangle_{\mathcal{T}} \equiv \sum_{\tau=0}^{\mathcal{T}}(\ldots)/\mathcal{T}$. In the FCT, after a time $\mathcal{T} > \tau_\phi$, the average global phase correlation function $\mathcal{C}_\phi(\mathcal{T})$, defined as

$$\mathcal{C}_\phi(\mathcal{T}) \equiv \frac{1}{N_f}\sum_{\delta\nu}|C_{\delta\nu}(\mathcal{T})| \tag{5}$$

$$C_{\delta\nu}(\mathcal{T}) = \frac{1}{N_f}\sum_{\nu}\langle\cos\left(\phi_\nu - \phi_{\nu+\delta\nu}\right)\rangle_{\mathcal{T}} \tag{6}$$

is observed to decay to zero. This is at difference with the NBT where, in the high power regime, $C_\phi(\mathcal{T})$ is finite also for $\mathcal{T} \to \infty$. For the FCT, the distribution of correlation times τ_ϕ as the optical power varies across the lasing threshold is sharply peaked around its logarithmic average $\overline{\ln \tau_\phi}$ below threshold, cf. Fig. 5. For increasing $\mathcal{P} > \mathcal{P}_c$ the distribution tends to a flat curve.

Vanishing two-mode correlators

A related phenomenon is that the average over $\mathcal{T} > \tau_\phi$ of two-mode phase correlations $C_{\delta\nu}(\mathcal{T})$, cf. Eq. (6),

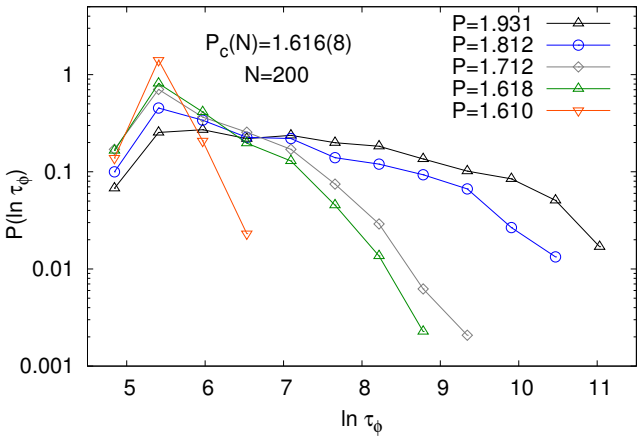

FIG. 5: (Color online) Distribution of the decay time of the equal time phase correlation function for a system of $N = N_f = 200$ modes across the threshold $\mathcal{P}_c(N = 200) = 1.616(8)$. Time τ in is Monte Carlo steps.

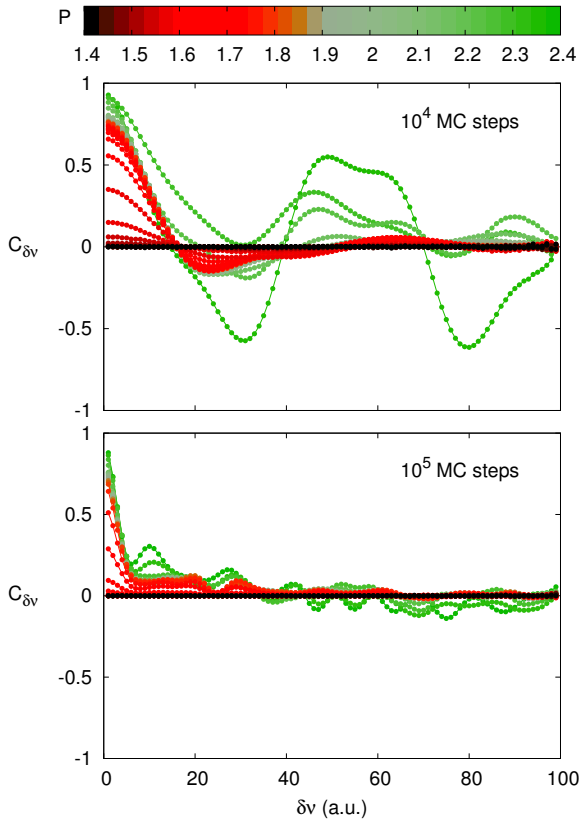

FIG. 6: (Color online) Phase-Phase correlation $C_{\delta\nu}(\mathcal{T})$ as function of frequency difference $\delta\nu = \nu' - \nu$ and optical power $\mathcal{P}$ for $\mathcal{T} = 10^4$ (top panel) and $\mathcal{T} = 10^5$ (bottom panel) in a FCT cavity with $N = 100$ and $N_q = \mathcal{O}(N^2)$. The threshold power is $\mathcal{P}_c(100) = 1.62(2)$ and the range of power of the displayed correlations is reported on the top palette from black (black online) for low power to light grey (light green online) for high power.

vanishes, as shown in Fig. 6, implying a zero ensemble average. This occurs though modes with frequencies ν, $\nu' = \nu + \delta\nu$ *are* correlated at each time τ , cf. bottom insets of Fig. 4, and $C_{\delta\nu}(\mathcal{T}) \neq 0$ when $\mathcal{T} \lesssim \tau_\phi$. In Fig. 6 we show $C_{\delta\nu}(\mathcal{T})$ as function of $\delta\nu = \nu' - \nu$ for $\mathcal{T} = 10^4$ and $\mathcal{T} = 10^5$. In the top panel, at shorter time window $\mathcal{T} = 10^4$, one clearly observes that $C_{\delta\nu}$ is completely uncorrelated independently of $\delta\nu$ for $\mathcal{P} < \mathcal{P}_c$. As the pumping increases above the threshold, $C_{\delta\nu}$ displays a non-trivial behavior as a function of $\delta\nu$. Above threshold, thus, the global phase correlation function $\mathcal{C}_\phi$, cf. Eq. (5), becomes larger the higher the pumping. In other words, the correlation time τ_ϕ grows with $\mathcal{P}$ and overcomes $\mathcal{T}$: $\tau_\phi(\mathcal{P} > \mathcal{P}_c) > 10^4$. In the bottom panel of Fig. 6 we consider, instead, a time window $\mathcal{T}$ larger than the average correlation time $\tau_\phi(\mathcal{P})$ for most of the simulated pumping values $\mathcal{P}$, cf. Fig. 5: it can be observed that $C_{\delta\nu}(10^5) \simeq 0$ for practically almost all $\delta\nu$, but the smallest ones for large power. The oscillations displayed by $C_{\delta\nu}(\mathcal{T})$ in Fig. 6 in the ML laser regime are due to the fact that different phase delays are involved in the thermal average. Indeed, cf. bottom insets of Fig. 4, the slope of $\phi(\nu)$ changes with time τ.

The origin of the vanishing of two-mode correlators is reminiscent of symmetry conservation in gauge lattice theories [24] and will be discussed elsewhere [23]. We just mention that the main difference in the lasing regime for the two topologies is that in the NBT the global $U(1)$ symmetry is spontaneously broken, whereas in the FCT it is conserved across the threshold.

V. CONCLUSIONS

We present the first statistical mechanical approach to the study of real-world ultrashort mode-locked multimode lasers in closed optical cavities, including possible degrees of topological disorder. In previous approaches, statistical mechanical systems with distinct resonances have been studied in the mean-field approximation, see, e. g., Refs. [14, 15, 25]. The key point is, though, that the mean field solution is exact only in the narrow bandwidth limit. When describing inhomogeneous topologies, such as the Frequency Comb Topology of equi-spaced well-refined resonances, the only thing that the mean-field theory can account for is a shift in the pumping threshold resulting from the dilution (in fact, just a modification of the coupling constant). The nature of the predicted mode-locked regime remains, indeed, identical to the one predicted assuming narrow band-width. This limit basically lies in the very definition of the mean-field method: since the fluctuations of the mode degrees of freedom are neglected a many-body problem is actually reduced to a one-body problem, in which all modes exhibit a common average phase and a common average intensity. The inhomogeneity in frequency dependence of the interaction network in more realistic cases, in which modes with near-by frequencies have stronger cou-

pling, is simply neglected by construction. Because of the mean-field assumption, previous approaches have not, and could not have, accounted for the main properties here reported: phase waves, non-equipartition threshold and vanishing two-mode correlators.

Our approach, going beyond mean-field theory, with Monte Carlo simulations of equilibrium dynamics, allows to reproduce and study the onset of the lasing regime and the behavior of emission spectra and laser pulses and relative group phase delays at any supplied power. The existence of metastable lasing regimes marked by spinodal points in the energy behavior, cf. inset of Fig. 1, accounts for the onset of optical bistability [26, 27]. The phenomenon of power condensation for extreme dilution of mode interaction and the vanishing of the equal time two-mode phase correlations for long times are properties that can be experimentally tested. Furthermore, this kind of approach opens the way to further analyze the carrier-envelop offset phase behavior, and the tolerance to disorder in the coupling SAM coefficient. The latter analysis is useful, e.g., for stabilized micro resonator in chip-based devices [28, 29] in which technical precision undergoes μm size constraints and controlling material damage is a true challenge. Eventually, including open cavity terms [30, 31] and strong disorder in the nonlinear coupling [3, 6–8], our approach can be applied to the study of random lasers [32–36].

Acknowledgements

The authors would like to thank Claudio Conti, Andrea Crisanti and Giorgio Parisi for stimulating discussions. The research leading to these results has received funding from the Italian Ministry of Education, University and Research under the Basic Research Investigation Fund (FIRB/2008) program/CINECA grant code RBFR08M3P4 and under the PRIN2010 program, grant code 2010HXAW77-008 and from the People Programme (Marie Curie Actions) of the European Union's Seventh Framework Programme FP7/2007-2013/ under REA grant agreement n 290038, NETADIS project.

VI. SUPPLEMENTAL MATERIAL

Spectra dynamics [Video 1]

In the file `Video1_spectral_dynamics.mpg` a video is shown for the dynamics of spectra $I(\lambda;\tau) = |a(\lambda;\tau)|^2$ for a FCT system with $N = N_f = 500$ modes and frequencies. The gain wavelength profile $g(\lambda)$ is taken uniform, i.e. $\sigma_g = \infty$. The finite size threshold for this specific system is $\mathcal{P}_c = 1.578(8)$. Dynamic sequences at three pumping rate are reported: in the incoherent CW regime ($\mathcal{P} = 1.308$), slightly above the lasing threshold ($\mathcal{P} = 1.865$) and for high pumping ($\mathcal{P} = 2.94$). Each MC step corresponds to the interval between two pulsed emissions in the mode-locked lasing regime. In the video each single frame is averaged over 10 subsequent Monte Carlo steps and frames are shown at intervals of 100 Monte Carlo steps.

Lasing pulse and phase delay dynamics [Video 2]

In the file `Video2_phase_delay_dynamycs.mpg` a video is shown for the stationary dynamics of the relationship $\phi(\nu)$ of lasing pulses in a simulation of a FCT system of $N = N_f = 500$ modes with an initial random dilution of $N_q^{\rm tot} = 37500000 = 0.3N^3$ and a final number of interacting quadruplets $N_q^{\rm FMC} = 49965$. The lasing system is at optical power $\mathcal{P} = 1.651$, right above the lasing threshold $\mathcal{P}_c = 1.578(8)$. The initial distribution of the gain among frequencies is taken as uniform. The interval between each frame is 100 Monte Carlo steps. It can be observed that at each time τ, corresponding to a pulsed emission, $\phi(\nu)$ is approximately linear, yielding a well defined phase delay ϕ' independent from ν. As the dynamics runs, though, $\phi'(\tau)$ changes, progressively taking a broad interval of values.

[1] H. A. Haus, IEEE J. Quantum Electron. **6**, 1173 (2000).
[2] H. A. Haus, *Waves and Fields in Optoelectronics* (Prentice-Hall, Englewood Cliffs, N. J., 1984).
[3] F. Antenucci, C. Conti, A. Crisanti, and L. Leuzzi, Phys. Rev. Lett. **114**, 043901 (2015).
[4] A. Marruzzo and L. Leuzzi, Phys. Rev. B **91**, 054201 (2015).
[5] A. Gordon and B. Fischer, Phys. Rev. Lett. **89**, 103901 (2002).
[6] L. Angelani, C. Conti, G. Ruocco, and F. Zamponi, Phys. Rev. Lett. **96**, 065702 (2006).
[7] L. Leuzzi, C. Conti, V. Folli, L. Angelani, and G. Ruocco, Phys. Rev. Lett. **102**, 083901 (2009).
[8] C. Conti and L. Leuzzi, Phys. Rev. B **83**, 134204 (2011).
[9] T. Udem, R. Holzwarth, and T. Hansch, Nature **416**, 233 (2002).
[10] A. Baltuška, T. Udem, M. Uiberacker, M. Hentschel, E. Goulielmakis, C. Gohle, R. Holzwarth, V. S. Yakovlev, A. Scrinzi, T. W. Hänsch, et al., Nature **421**, 611 (2003).
[11] A. Schliesser, C. Gohle, and T. W. Udem, Th. an Hänsch, Optics Express **14**, 5975 (2006).
[12] T. Brabec and F. Krausz, Rev. Mod. Phys. **72**, 545 (2000).
[13] Murray Sargent III, Marlan O'Scully and Willis E. Lamb, *Laser Physics* (Addison Wesley Publishing Company, 1978).
[14] A. Gordon and B. Fischer, Opt. Comm. **223**, 151 (2003).
[15] O. Gat, A. Gordon, and B. Fischer, Phys. Rev. E **70**,

046108 (2004).
[16] M. Bellini and T. W. Hansch, Opt.Lett. **25**, 1049 (2000).
[17] S. A. Diddams, D. J. Jones, J. Ye, S. T. Cundiff, J. L. Hall, J. K. Ranka, R. S. Windeler, R. Holzwarth, T. Udem, and T. W. Hansch, Phys. Rev. Lett. **84**, 5102 (2000).
[18] K. Hukushima and K. Nemoto, J. Phys. Soc. Japan **65**, 1604 (1996).
[19] P. Peretto, Biological Cybernetics **50**, 51 (1984).
[20] H. Mahmoudi and D. Saad, J. Stat. Mech. **2014**, P07001 (2014).
[21] F. L. Metz and W. K. Theumann, J. Phys. A **41**, 265001 (2008).
[22] F. L. Metz and W. K. Theumann, J. Phys. A **42**, 385001 (2009).
[23] F. Antenucci, M. Ibañez Berganza, and L. Leuzzi, arXiv:1412.8610 (2014).
[24] J. B. Kogut, Rev. Mod. Phys. **51**, 659 (1979).
[25] A. Rosen, R. Weill, B. Levit, V. Smulakovsky, A. Bekker, and B. Fischer, Phys. Rev. Lett. **105**, 013905 (2010).
[26] H. Gibbs, *Optical Bistability: Controlling Light with Light* (Elsevier (Amsterdam), 1985).
[27] A. Baas, J. P. Karr, H. Eleuch, and E. Giacobino, Phys. Rev. A **69**, 023809 (2004).
[28] C.-C. Lee, I. Hartl, C. Mohr, J. Bethge, S. Suzuki, M. E. Fermann, and T. R. Schibli, Opt. Lett. **37**, 3084 (2012).
[29] K. Saha, Y. Okawachi, S. Bonggu, J. S. Levy, R. Salem, A. R. Johnson, M. A. Foster, M. Lamont, M. Lipson, and A. L. Gaeta, Opt. Exp. **21**, 1335 (2013).
[30] C. Viviescas and G. Hackenbroich, Phys. Rev. A **67**, 013805 (2003).
[31] G. Hackenbroich, C. Viviescas, and F. Haake, Phys. Rev. A **68**, 063805 (2003).
[32] N. M. Lawandy, R. M. Balachandran, A. S. L. Gomes, and E. Sauvain, Nature **368**, 436 (1994).
[33] H. Cao, Y. G. Zhao, H. C. Ong, S. T. Ho, J. Y. Dai, J. Y. Wu, and R. P. H. Chang, Appl. Phys. Lett. **73**, 3656 (1998).
[34] H. Cao, J. Phys. A. : Math. Gen. **38**, 10497 (2005).
[35] D. S. Wiersma, Nature Physics **4**, 359 (2008).
[36] N. Ghofraniha, I. Viola, F. Di Maria, G. Barbarella, G. Gigli, L. Leuzzi, and C. Conti, Nat. Commun. **6**, 6058 (2015).
[37] Supplemental Material (2015).
[38] The three orderings inequivalent with respect to the FMC are $\{k_1, k_2, k_3, k_4\}$, $\{k_1, k_3, k_2, k_4\}$ and $\{k_1, k_4, k_2, k_3\}$. Given a quadruplet $\{A, B, C, D\}$ the equivalent permutations are (i): $A \leftrightarrow C$, (ii): $B \leftrightarrow D$, (iii): $A \leftrightarrow B$ & $C \leftrightarrow D$ and their combinations.
[39] We also tested the network-to-network fluctuations over different numbers of network realizations finding that the fluctuations $[\overline{O^2} - \overline{O}^2]^{1/2}$ of any obserables O over the distribution of topologies are one order of magnitude lower than thermal fluctuations, $[\langle O^2\rangle - \langle O\rangle^2]^{1/2}$, already in the worst case of small size $N = 100$.